Classification of Cape Gooseberry Fruit According to Its Level of Ripeness Using Machine Learning Techniques and Different Color Spaces

**WILSON CASTRO[1], JIMY OBLITAS[2], MIGUEL DE-LA-TORRE[3], CARLOS COTRINA[1],
KAREN BAZÁN[1], AND HIMER AVILA-GEORGE [3], (Senior Member, IEEE)**

[1]Facultad de Ingeniería, Universidad Privada del Norte, Cajamarca 06002, Peru
[2]Departamento de Tecnología de Alimentos, Universidad de Lleida, 25198 Lleida, Spain
[3]Centro Universitario de los Valles, Universidad de Guadalajara, Ameca 46600, Mexico

Coorresponding author: Himer Avila-George (himer.avila@academicos.udg.mx)

ABSTRACT The classification of fresh fruits according to their visual ripeness is typically a subjective and tedious task; consequently, there is a growing interest in the use of non-contact techniques to automate this process. Machine learning techniques, such as artificial neural networks, support vector machines (SVMs), decision trees, and K-nearest neighbor algorithms, have been successfully applied for classification problems in the literature, particularly for images of fruit. However, the particularities of each classification problem make it difficult, if not impossible, to select a general technique that is applicable to all types of fruit. In this paper, the combinations of four machine learning techniques and three color spaces (*RGB*, *HSV*, and *L*a*b**) were evaluated with regard to their ability to classify Cape gooseberry fruits. To this end, 925 Cape gooseberry fruit samples were collected, and each fruit was manually classified into one of seven different classes according to its level of ripeness. The color values of each fruit image in the three color spaces and their corresponding ripening stages were organized for training and validation following a fivefold cross-validation strategy in an iterative process repeated 100 times. According to the results, the classification of Cape gooseberry fruits by their ripeness level was sensitive to both the color space and the classification technique used. The models based on the *L*a*b** color space and the SVM classifier showed the highest f-measure regardless of the color space, and the principal component analysis combination of color spaces improved the performance of the models at the expense of increased complexity.

INDEX TERMS Cape gooseberry, artificial neural networks, support vector machines, decision trees, K-nearest neighbors, color spaces, PCA, multiclass confusion matrix.

I. INTRODUCTION

The Cape gooseberry (*Physalis peruviana L.*), known as the goldenberry in English-speaking countries and as aguaymanto in Peru, is a plant native to the South American Andes [1], [2]. This plant has attracted the interest of functional food markets (emerging markets of growing economic importance) due to its medicinal, nutritious, and pharmaceutical properties [3]–[5]. Because the food industry needs to provide fruits with a high and consistent quality, it is necessary to improve their production methods to ensure that only high-quality fruits are retained during manufacturing and commercialization [6].

The associate editor coordinating the review of this manuscript and approving it for publication was Tao Zhou.

An important step in ensuring a high quality for fresh fruits such as the Cape gooseberry is sorting, which is currently based on the visual inspection of color, size, and shape parameters [7]. However, the visual inspection process suffers from certain disadvantages: it is subjective, variable, tedious, laborious, inconsistent and easily influenced by the environment [8]. Consequently, there is growing interest in reducing the subjectivity of visual inspection using innovative and non-contact measurements such as artificial vision systems, which can measure the entire surface of a sample; as a result, these types of systems are more representative than colorimeters, which are based on point-to-point measurements [9]–[12].

Computer vision systems *(CVSs)* are currently employed for the classification of horticultural products and for

monitoring such products for defects and bruising [10]. At present, the development of CVSs is focused on defining new methods for the evaluation of color and shape parameters. In this context, color is of special interest because it constitutes an important sensory attribute providing necessary quality information for human perception. In particular, consumers tend to prefer products exhibiting a uniform appearance and vivid colors. Moreover, color has been closely associated with various quality factors (ripeness, variety, and desirability) and food safety. Therefore, color is an essential classification element for most food products [13]–[16].

Each color that humans can recognize in an image is formed from a combination of the three so-called primary colors, *red, green,* and *blue*, which can be arranged within a color space to facilitate the specification of colors in a standardized and widely accepted form. In essence, a color space is the specification of a three-dimensional coordinate system and a subspace of this system in which a single point represents each color. Nevertheless, there is more than one color space, and each color space can be classified into one of three spaces according to [16]: hardware-oriented spaces, human-oriented spaces, and instrumental spaces.

- *Hardware-oriented spaces*. These color spaces are defined based on the properties of the hardware devices used to reproduce the colors. In this category, the most popular color spaces are *RGB*, *YIQ*, and *CMYK*.
- *Human-oriented spaces*. These color spaces are based on hue and saturation. The most popular color spaces in this category are *HSI*, *HSL*, *HSV* and *HSB*. These spaces correspond to the concepts of tint, shade, and tone, which are specified by an artist based on inherent color characteristics. However, as with human vision, human-oriented spaces are not sensitive to small variations in color and are therefore not suitable for evaluating changes in the color of a product during processing.
- *Instrumental spaces*. Color spaces such as *XYZ, L*a*b*,* and *L*u*v** are used for color instruments. Unlike hardware-oriented spaces, in which various output media have different coordinates for the same color, the color coordinates of an instrumental space are the same on all output media.

The main features of the color parameters based on the works of [17] and [18] are detailed in Table 1, which shows that each color space was developed for a particular purpose; as a result, each color space has certain advantages when used in classification and identification problems.

Thus, although *CVSs* directly provide information in the *RGB* space, some works, such as that of Du and Sun [19], have aimed to determine whether any differences in the classification are caused by the selected color space or by the utilized segmentation technique.

According to [16], "In the color measurement of food, the *L*a*b** color space is the most commonly used due to the uniform distribution of colors and because it is perceptually uniform."

TABLE 1. Color parameters used for classification.

Space	Parameter	Description
RGB	R	Red measured in digital image [0, 255]
	G	Green measured in digital image [0, 255]
	B	Blue measured in digital image [0, 255]
HSV	H	Hue derived from *RGB* [0, 360]
	S	Saturation derived from *RGB* [0, 100]
	V	Value derived from *RGB* [0, 100]
L*a*b*	L*	Luminosity derived from *RGB* [0, 100]
	a*	Red/green opposing colors [-128, 127]
	b*	Yellow/blue opposing colors [-128, 127]

TABLE 2. Fruit/vegetable ripening evaluations using expert system techniques in different color spaces.

Item	Color space	Processing method	Accuracy	Ref.
Apple	HSI	SVM	95	[22]
Apple	*L*a*b**	MDA	100	[23]
Avocado	*RGB*	K-Means	82.22	[24]
Banana	*L*a*b**	LDA	98	[25]
Banana	*RGB*	ANN	96	[26]
Blueberry	*RGB*	KNN and SK-Means	85-98	[27]
Date	*RGB*	K-Means	99.6	[28]
Lime	*RGB*	ANN	100	[29]
Mango	*RGB*	SVM	96	[30]
Mango	*L*a*b** and HSB	MDA	90	[31]
Mango	*L*a*b**	LS-SVM	88	[32]
Oil palm	*L*a*b**	ANN	91.67	[33]
Pepper	*HSV*	SVM	93.89	[34]
Persimmon	*RGB* + *L*a*b**	QDA	90.24	[35]
Tomato	HSV	SVM	90.8	[36]
Tomato	*RGB*	DT	94.29	[37]
Tomato	*RGB*	LDA	81	[38]
Tomato	*L*a*b**	ANN	96	[39]
Watermelon	YCbCr	ANN	86.51	[40]

In image analysis, several pattern recognition techniques can be used; however, supervised methods are the most popular. Supervised learning is an automatic learning task that infers a function given labeled training data. In the fruit inspection industry, the support vector machine *(SVM)*, k-nearest neighbor *(KNN)*, artificial neural network *(ANN)*, and decision tree *(DT)* pattern classification methods are between the most common [20], [21].

The use of *CVSs* to determine the level of ripeness has been studied for a variety of fruits, including apples, bananas, blueberries, dates, mangoes, and tomatoes. Table 2 summarizes the main findings of investigations on fruit ripening stages using *CVSs*. Evidently, distinct approaches have combined different color spaces with a variety of classification algorithms; in general, however, these techniques have explored only one or two combinations to select the approach with the highest accuracy. Additionally, for the Cape gooseberry, the use of image analysis to classify the ripening stage has not been reported.

Thus, we present a study for classifying Cape gooseberry fruits using different color spaces and four of the leading supervised learning techniques. The principal objective is to determine which color space and which classification method

are the most appropriate for classifying Cape gooseberry fruits according to their ripening stage.

II. MATERIALS AND METHODS

A. CAPE GOOSEBERRY FRUIT SAMPLES

A sample of gooseberry fruits was collected from a plantation located in the village of El Faro, Celendin Province, Cajamarca, Peru [UTM: −6.906469, −78.257071]. The sample consisted of 925 Cape gooseberry fruits with different levels of ripeness.

B. COMPUTER VISION SYSTEM FOR CLASSIFYING CAPE GOOSEBERRIES

The hardware and software that constitute this system are described below.

- *Conveyor belt*. The conveyor belt is 160 cm long, 25 cm wide, and 80 cm high. The speed is adjustable, and the conveyor is operated by an EPLI motor (MS 632-4 60 Hz, 0.18 KW, 0.25 HP, 220 V, 1570 RPM).
- *VGA webcam*. The utilized webcam has the following specifications:
  - Trademark: Halion
  - Model: HA-411
  - Resolution: 1280x720 pixels

  The webcam was located 35 cm above the sample.
  The internal walls of the *CVS* were painted black to avoid light leakage and exterior reflections of the room in a method similar to that realized by Pedreschi *et al.* [41].
- *Lightning source*. A directional lighting system composed of two long fluorescent tubes (Philips TL-D Super, cold daylight, 80 cm, 36 W) distributed symmetrically on both sides of the sample was used, and a circular fluorescent tube (Philips GX23 PH-T9, cold daylight, 21.6 cm, 22 W) was located at the top.
- *Computer*. We used a laptop (Intel(R) Pentium(R) Dual-Core CPU T4200 @ 2.00 GHz and 3.0 GB RAM).
- *Informatics tool for data acquisition*. A computer tool was developed to control the acquisition of the images and their subsequent analysis. This tool was implemented using Matlab.

C. METHODOLOGY

The research methodology, which was based on [42], is shown in Figure 1. In general, data were first extracted from image samples to obtain feature vectors organized by each class and vector space. Then, four classification models were trained and tested using a cross-validation strategy with one hundred iterations. Finally, the results were statistically evaluated to analyze the effects of the different color spaces on the performances of the four classifiers.

The methodology employed in this study is described in detail in the subsequent sections.

1) DATA EXTRACTION

In this step, information on the color parameters in three color spaces was collected from each fruit in the sample; for
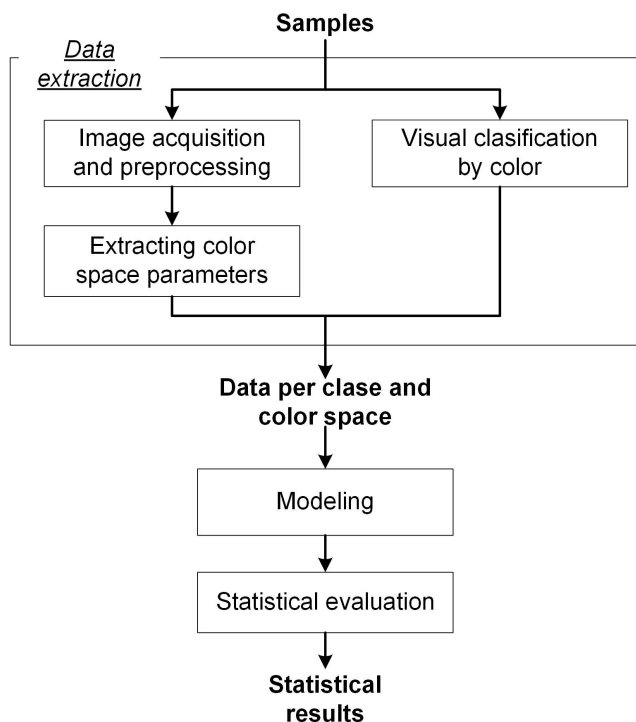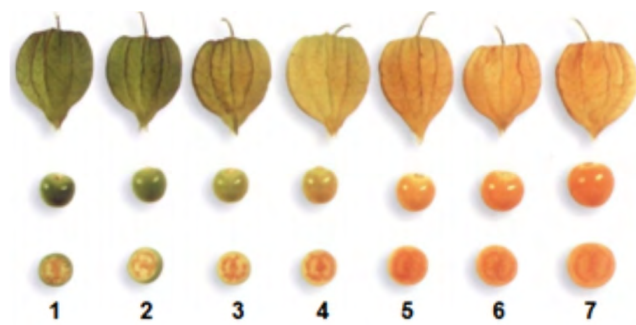

FIGURE 1. Experimental methodology.

FIGURE 2. Ripeness states of Cape gooseberry.

this step, each fruit was visually classified according to its ripeness level.

a: VISUAL CLASSIFICATION BY COLOR

Fruit images were classified into seven different levels according to the ripening stage, similar to the method used by Bravo and Osorio [43]. The surface color was used for the classification as indicated by the NTC 4580 (Colombian Technical Normative) standard for Cape gooseberry, and the visual scale proposed by Fischer *et al.* [44] was employed (see Figure 2).

For the visual classification, 5 expert judges labeled each fruit image, and their decisions were reached by a majority vote.

b: IMAGE ACQUISITION AND PREPROCESSING

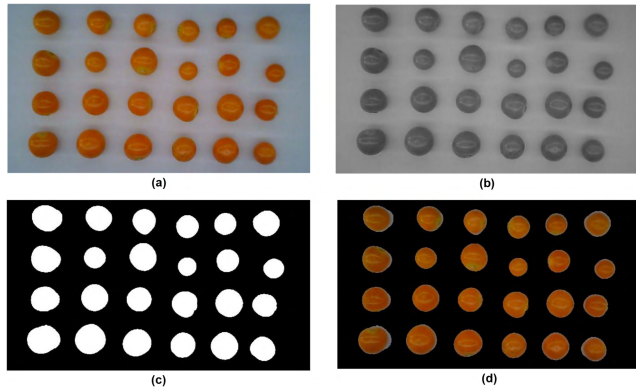The steps in this stage were based on the image processing techniques proposed by Arakeri and Laksmana [8],

FIGURE 3. Images of the acquisition and preprocessing stages.

as detailed below:

- *Locations of samples*. Fruits for each class determined in the previous step were placed on the conveyor belt and then organized in a grid-like arrangement with four rows and five to seven columns. The fruits were successively displayed on the conveyor belt until the entire set was presented to the system.
- *Image acquisition*. Fruits were conveyed to the corresponding area for image acquisition. The software component discussed in Section II-B was used to capture the images, and each image was stored (see Figure 3(a)) according to the corresponding class.
- *Image enhancement*. Sample images were enhanced by utilizing the Gaussian filter shown in Eq. 1 to smooth visual artifacts that appeared due to either lighting conditions or fruit deterioration. Figure 3(b) shows the resulting images.

$$g(x, y) = \frac{1}{2\pi\sigma} e^{\frac{-(x^2+y^2)}{2\sigma^2}}, \qquad (1)$$

where

$$g = \text{Filtered image},$$
$$(x, y) = \text{Position of pixel},$$
$$\sigma = \text{Standard deviation of the Gaussian filter}.$$

- *Segmentation*. Fruit images were converted into grayscale images, as shown in Figure 3(c), and the threshold segmentation approach based on Eq. 2 was used. In the resulting images, the samples were isolated from the background, and their pixels were consequently identified, as shown in Figure 3(d).

$$h(x, y) = \begin{cases} 1 & \text{if } g(x, y) \geq T \\ 0 & \text{if } g(x, y) < T \end{cases} \qquad (2)$$

where

$$h = \text{Segmented image},$$
$$(x, y) = \text{Position of pixel},$$
$$T = \text{Threshold value}.$$

c: EXTRACTING COLOR SPACE PARAMETERS

From each region of fruit in the segmented images shown in Figure 3(d), the mean values of the color parameters in the *RGB* color space were determined similar to the work of Blasco *et al.* [45]. Then, these mean values were converted into the *HSV* and *L*a*b** color spaces using standard conversion methods (e.g., those implemented in packages such as *rgb2hsv* and *rgb2lab* in Matlab). These values, all of which were linked to each fruit in the different classes, were stored in a database for subsequent modeling.

2) MODELING

The dataset obtained from the 925 evaluated fruits was used to construct the models and subsequently validate them. This dataset was randomly divided into modeling and validation datasets using a 5-fold cross-validation strategy for each model and space color combination; this process was performed one hundred times to test its reproducibility.
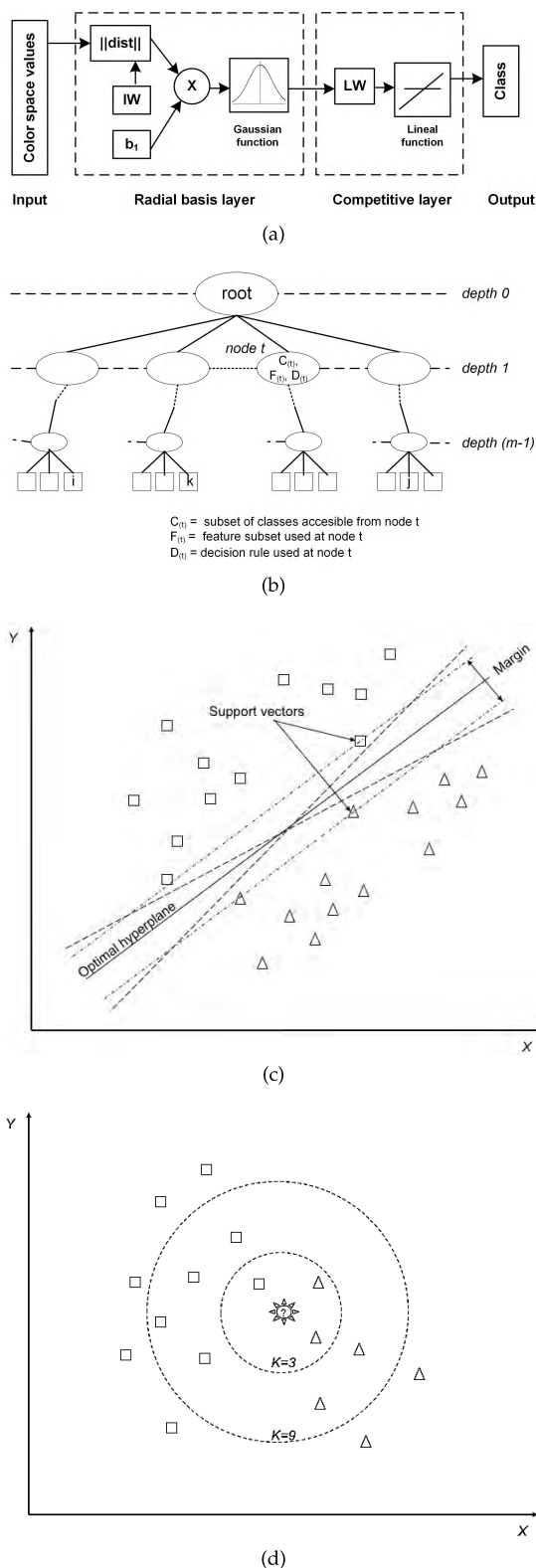
In this step, four supervised machine learning techniques were used for modeling. Each of these techniques considers the categorical labels when data entries $x_1, x_2, \ldots, x_n$ must be assigned to predefined classes $C_1, C_2, \ldots, C_m$; in multiclass classification, the input is to be classified into only one of n non-overlapping classes. Below, each supervised machine learning technique is described.

a: ANN

This nonlinear supervised classification method uses mathematical models to simulate biological neural networks. A common type of *ANN* is the radial basis function *ANN* (RBF-ANN), which is used to classify features into different classes by finding common characteristics among the samples of the known feature class. In this type of network, nonlinearity is embedded within the transfer functions of the hidden layer neurons, making the optimization of tunable parameters a linear search [46], [47]. Figure 4(a) shows a schematic representation of the RBF-ANN, which was proposed by Beale *et al.* [48]. Matlab's Neural Network Toolbox was used to implement the classification models based on the ANN technique. Particularly, we used the *newpnn* function to create and train probabilistic neural networks, which are a kind of radial basis network, and the *sim* function was used for the simulation stage.

b: DT

This technique is a tree-based exemplification of the knowledge used to represent classification rules. The internal nodes of a tree represent tests of an attribute; each branch represents the outcome of the test, and the leaf nodes represent class labels. Traversing a branch from the root node to a leaf node decodes the information enclosed in the form of if-then statements, and each branch leads to a single rule. Figure 4(b) shows a schematic of this technique, which was proposed by Safavian and Landgrebe [49]. Therefore, *DTs* can be exploited to automatically generate the classification

(a)

(b)

$C_{(t)}$ = subset of classes accesible from node t
$F_{(t)}$ = feature subset used at node t
$D_{(t)}$ = decision rule used at node t

(c)

(d)

FIGURE 4. Four supervised machine learning techniques used in this work for modeling. (a) Generalized RBF-ANN structure; (b) generalized DT structure; (c) SVM example; and (d) KNN example.

rules without requiring a human expert [37], [49]. To create the classifier based on the DT technique, Matlab's Machine Learning Toolbox *(MLT)*, which uses the standard

classification and regression trees *(CART)* algorithm to create DTs [50], was used. For fitting and training, the multiclass classifier function *fitctree* and *predict* functions were used.

c: SVM

The SVM classifier is a supervised nonparametric statistical learning technique that is widely used for classification by constructing a hyperplane or a set of hyperplanes in a high-dimensional space [22], [30]. Figure 4(c) shows the support vectors and the hyperplane separating two classes, which are defined by squares and triangles. In this case, the *fitcecoc* fitting function and the *predict* function were used; both functions were implemented in Matlab's MLT. We also used a linear kernel and tuned the classifier using Bayesian optimization.

d: KNN

The KNN algorithm is a nonparametric classification technique cache of all the training data that predicts the response of a new sample by analyzing a certain number of the nearest neighbors in the feature space of the sample [28], [51]. Figure 4(d) shows an example of this technique; the element to be classified is the sun symbol. For $k = 3$, this object is classified as the triangle class since only one square and two triangles are inside the circle that contains them. If $k = 9$, this object is classified as the square class since there are four triangles and five squares inside the outer circle. To create the classifier based on the *KNN* technique, Matlab's MLT was used; the *fitcknn* function was used to train the model, and the *predict* function was used to predict the labels. Finally, Bayesian optimization was used to tune *KNN* classifier.

3) STATISTICAL EVALUATION

After obtaining the class predictions, the performance of each combination of classifier and color space was determined using a confusion matrix. This technique, which contains information about the actual and predicted ratings obtained by a classification system, is one of the most common approaches used within the machine learning community.

A confusion matrix has two dimensions (real and predicted classes). Each row represents the instances of a real class, whereas each column represents the cases of a predicted class. Table 3 shows the basic form of the confusion matrix for a multiclass classification problem. The element N_{ij} of the confusion matrix represents the number of samples that belong to class C_i but that are classified as class C_j.

Some performance measures, namely, the *accuracy*, *precision*, *recall* and *f-measure*, can be defined from the information contained in a confusion matrix. These measures are determined by the numbers of classification errors and hits made by the classifier. Table 3b illustrates the intuition behind these performance measures based on a class-specific classification for class C_i. In this sense, *positive* samples correspond to the ith class, and *negative* samples correspond to all other classes, whereas *true* and *false* terms refer to samples either correctly or incorrectly classified, respectively.

TABLE 3. (a) Generalized confusion matrix for several classes. (b) Class-specific performance measures according to their definitions based on the confusion matrix.

(a)

		Predicted class (C_j)				
		C_1	...	C_j	...	C_n
Actual class (C_i)	C_1	$N_{1,1}$	...	$N_{1,j}$	...	$N_{1,n}$
	$\vdots$	$\vdots$	$\vdots$	$\vdots$	$\vdots$	$\vdots$
	C_i	$N_{i,1}$	...	$N_{i,j}$	...	$N_{i,n}$
	$\vdots$	$\vdots$	$\vdots$	$\vdots$	$\vdots$	$\vdots$
	C_n	$N_{n,1}$	...	$N_{n,j}$	...	$N_{n,n}$

(b)

		Predicted class (C_j)				
		$\hat{C}_1$	...	$\hat{C}_i$	...	$\hat{C}_n$
Actual class (C_i)	C_1	TN_i	TN_i	$\mathbf{FP_i}$	TN_i	TN_i
	$\vdots$	TN_i	TN_i	$\mathbf{FP_i}$	TN_i	TN_i
	C_i	$\mathbf{FN_i}$	$\mathbf{FN_i}$	$\mathbf{TP_i}$	$\mathbf{FN_i}$	$\mathbf{FN_i}$
	$\vdots$	TN_i	TN_i	$\mathbf{FP_i}$	TN_i	TN_i
	C_n	TN_i	TN_i	$\mathbf{FP_i}$	TN_i	TN_i

The performance measures derived from Table 3b that were employed to evaluate the experimental results are described below.

TP$_\mathbf{i}$ True Positives. Amount of samples from class i that were correctly classified as positives (i.e., i classified as i); see Eq. 3.

$$TP_i = N_{ii} \qquad (3)$$

TN$_\mathbf{i}$ True Negatives. Amount of samples from class not-i that were correctly classified as negatives (i.e., correctly classified as not i); see Eq. 4.

$$TN_i = \sum_{j,k \neq i} N_{jk} = \sum_{j=1}^{n}\sum_{k=1}^{n} N_{jk} - (TP_i + FP_i + FN_i) \qquad (4)$$

FP$_\mathbf{i}$ False Positives. Amount of samples from class not-i that were wrongly classified as positives (i.e., incorrectly classified as class i); see Eq. 5.

$$FP_i = \sum_{k \neq i} N_{ki} = \sum_{k=1}^{n} N_{ki} - TP_i \qquad (5)$$

FN$_\mathbf{i}$ False Negatives. Amount of samples from class i that were wrongly classified as negatives (i.e., classified as any class except class i); see Eq. 6.

$$FN_i = \sum_{k \neq i} N_{ik} = \sum_{k=1}^{n} N_{ik} - TP_i \qquad (6)$$

The definitions of typical performance measures in terms of the above descriptions are defined in the literature. According to [52], the *accuracy* of a multiclass classifier defined by Eq. 7 is the proportion of the total number of correct predictions.

$$Accuracy = \frac{\sum_{i=1}^{n} TP_i}{\sum_{i=1}^{n}\sum_{j=1}^{n} N_{ij}} \qquad (7)$$

The *precision* defined by Eq. 8 is the amount of samples from class C_i that were correctly classified with respect to the samples that were predicted as positives by the classifier.

$$Precision_i = \frac{TP_i}{TP_i + FP_i} \qquad (8)$$

The *recall* or true positive rate (*tpr*) defined by Eq. 9 is a measure of the ability of a classifier to correctly select instances of the target class (C_i) related to the positive samples.

$$Recall_i = \frac{TP_i}{TP_i + FN_i} \qquad (9)$$

Finally, the *f-measure* is the harmonic mean of the precision and recall and is defined by Eq. 10.

$$F\text{-}Measure_i = 2 \times \frac{Precision_i \times Recall_i}{Precision_i + Recall_i} \qquad (10)$$
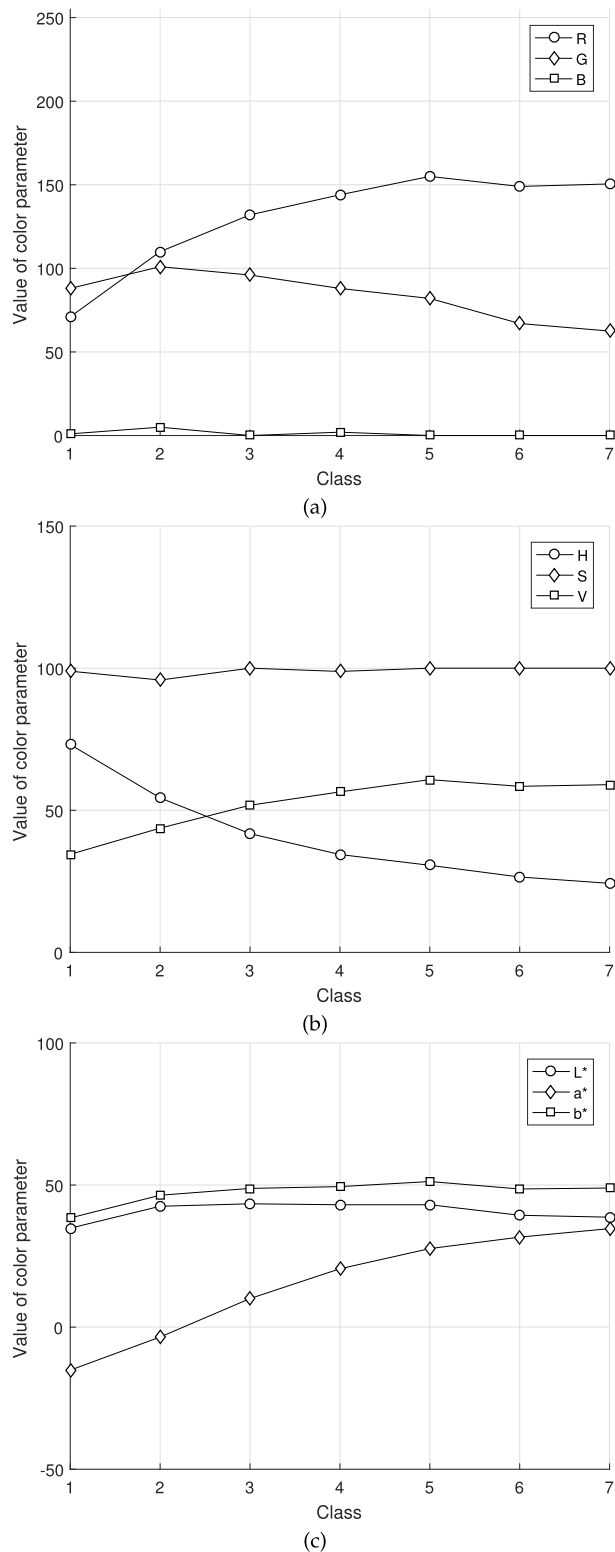
These four performance measures were computed after classifying the degree of ripening for each Cape gooseberry fruit to measure the influence of the color space on the classification. The color spaces employed for the comparison using principal component analysis *(PCA)* included the *RGB*, *HSV*, and *L*a*b** color spaces in addition to a fusion of all three. Four classification techniques were employed, namely, the *ANN*, *DT*, *SVM*, and *KNN* classifiers, and each of the sixteen combinations of color parameters and classifiers were compared by employing the performance measures defined in Eqs. 7-10. However, in this work, the *f-measure* was regarded as the main performance measure for the analysis due to its capacity to summarize the positive precision and recall in a single number; nevertheless, the accuracy was also reported to facilitate a comparison with the results reported in the literature.

III. RESULTS
A. CAPE GOOSEBERRY COLOR DURING RIPENING
Figure 5 shows the distribution of pixels for each class using the median color parameter values in all fruit images for each color space. As observed in Figure 5(a), the parameter R presents an upward trend throughout the ripening process with a starting value of 75 that increases to a maximum value of 150. In contrast, the parameter G begins at 89 and ends at 63, and the parameter B shows slight variability between 0 and 45.

For the *HSV* color space, Figure 5(b) shows that the parameter H exhibits a downward trend starting at 73 and ending at 24. The parameter S shows little variability with mean values

FIGURE 5. Median color parameter values of Cape gooseberry fruits at seven different ripening stages. (a) *RGB*; (b) *HSV*; and (c) *L*a*b**.

TABLE 4. Mean color parameters for the *L*a*b** color space at different ripening stages.

Parameter	Obtained	Source	
		[5]	[54]
L^*	38.69 ± 3.23	54.04 ± 0.34	71.37 ± 1.10
a^*	34.66 ± 3.11	23.67 ± 0.30	15.20 ± 0.48
b^*	48.95 ± 3.10	59.85 ± 0.29	61.76 ± 1.34

Mean $\pm$ standard deviation.

Concerning the $L^*a^*b^*$ color space, Figure 5(c) shows that the parameter L^* presents slight variability with values oscillating between 34 and 38. The parameter a^* exhibits an upward trend that starts at -15 and reaches a maximum of 34. Finally, the parameter b^* fluctuates between 38 and 51.

As explained in [23] and [53], changes in the parameters L^*, a^* and b^* are associated with increases in carotenoid levels and a loss of chlorophyll in the pericarp. Table 4 shows a comparison of the mean values for the $L^*a^*b^*$ space obtained in this work with those reported by Vásquez-Parra et al. [5] and Puente et al. [54].

B. MODEL EVALUATION

Figure 6 depicts the confusion matrices that summarize the average performance of each model (i.e., each pair of a classifier with a color space). A high prediction percentage for class C_i as class C_j is represented as a light gray, where i is the correct label and j is the predicted class. The white color in cell $N_{i,j}$ indicates that 100% of the predictions for class C_i are presented as class C_j. On the other hand, dark cells represent a lower percentage of predictions for class C_i as class C_j (black indicates a 0% prediction level).

In general, Figure 6 provides evidence that classes C_1 through C_4 are correctly classified by almost all the classifiers, while most of the errors appear in classes $C_5 - C_7$. This suggests that the classification of fruits with low levels of ripeness (one through four) is easier than that of fruits at a later ripening stage.

In the case of the ANN classifier, Figures 6(a-c) show that classes $C_2 - C_4$ are correctly classified in most cases (lighter colors in the diagonal), and only a few misclassifications are observed for classes C_1 and $C_5 - C_7$. However, in the $L^*a^*b^*$ color space, class C_1 is also correctly classified. This suggests that the $L^*a^*b^*$ color space facilitates the classification of class C_1 with the ANN classifier.

The confusion matrices for the DT and KNN classifiers shown in Figures 6(d-f) and (j-i) illustrate that it is consistently difficult for these two techniques to discriminate between classes C_5 and C_7 in any of the color spaces. In contrast, a relatively constant accuracy over all levels of ripeness is retrieved by the different combinations of the SVM classifier with the three color spaces.

Figure 7 summarizes the performance of each of the twelve classification models in terms of the f-measure. According to Figure 7, the SVM classifier exhibited the best results (f-measure $= 70.14 \pm 1.27\%$) in the $L^*a^*b^*$ color space, while the ANN classifier achieved the worst performance
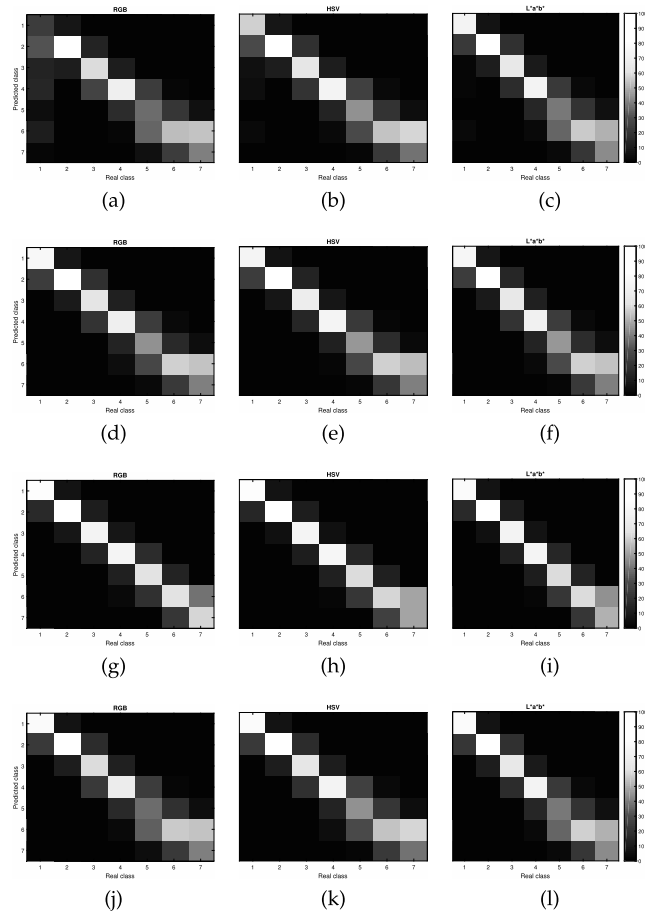
fluctuating between 98 and 100. Finally, the parameter V exhibits an upward trend throughout the maturation process with a minimum value of 34 and a maximum of 59.

FIGURE 6. Confusion matrices. (a-c) ANN; (d-f) DT; (g-i) SVM; and (j-l) KNN.

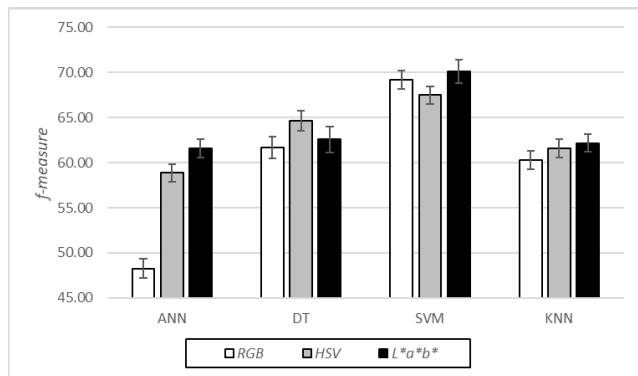**FIGURE 7.** Average *f-measure* for each classifier tested on the three color spaces.

(*f-measure* = 48.25 ± 1.07%) in the *RGB* color space. Likewise, for all the combinations, the effect of a different color space on the model performance was more evident for the ANN classifier. The models based on the *KNN* and *DT* techniques yielded good results regardless of the color space used (*f-measure* > 60%); between these two techniques, the *DT* model obtained slightly better results.

From these results, it is evident that every color space poses a distinct classification problem to each classifier.
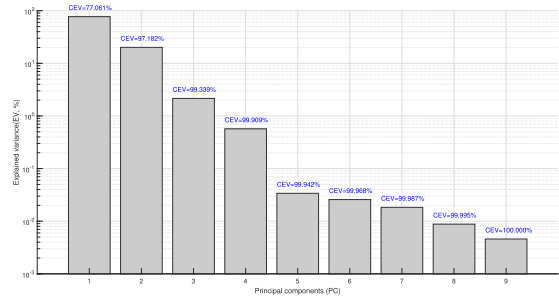

FIGURE 8. Amount of variance explained by each PC. CEV stands for cumulative explained variance.

Some classifiers (i.e., the ANN, SVM and KNN) perform better in the *L*a*b** color space, whereas others (i.e., the DT algorithm) take advantage of the sample distribution in the *HSV* color space. A further improvement in the performance was explored using a strategy of information fusion to combine the color parameters from all color spaces through *(PCA)*. This strategy allows the parameters from the three color spaces to be projected over $n < m$ principal components *(PCs)*, where $m = 9$ is the number of color parameters following the concatenation of parameters from all three color spaces.

According to the PCA performed over the three color spaces, the first three PCs can explain 99.339% of the variance. However, additional information useful for the classification is still provided by components 4 through 9, as shown in Figure 8 and demonstrated by the performance analysis.

Table 5 presents the performance of each classifier with respect to their combinations with the three distinct color spaces using *PCA* in terms of both the *accuracy* and the *f-measure*. Although the SVM classifier exhibits the best performance in the *L*a*b** color space, the PCA-based classifier shows a performance increase close to 2% in terms of the *f-measure* with an accuracy of 93.02% ± 0.19%. The *ANN*, *SVM* and *KNN* classifiers also display consistent increases in their performance in terms of either the *f-measure* or the *accuracy* as the PCs are augmented. However, the *DT* classifier exhibits a decrease in terms of the *f-measure*; this reduction may be due to the suboptimal tuning of hyperparameters, and thus, other optimization strategies may be suitable for the classification of Cape gooseberry fruits according to their level of ripeness.

Figure 9 illustrates the average performances of the four classifiers combined with the three color spaces in terms of the *f-measure* through PCA considering $n = \{1 \ldots m\}$ PCs. As expected, a single PC provides the worst average performance (with an *f-measure* close to 41%). However, as the feature space increased with the addition of PCs, the performance also increased, showing a simultaneous increase in the variability (as evidenced by the large error bars). This variability was generated by the differences in the performance between distinct classifiers, as shown in Table 5.

Finally, to complete the performance analysis, the receiver operating characteristic (ROC) curve was computed for each

TABLE 5. Average performance of each model in terms of the (a) *accuracy* and (b) *f-measure*. Bold numbers represent the highest performance achieved by each classifier.

(a)

	ANN		DT		SVM		KNN	
	Accuracy	*Stdev*	*Accuracy*	*Stdev*	*Accuracy*	*Stdev*	*Accuracy*	*Stdev*
RGB	85.90	0.29	89.94	0.32	92.47	0.20	89.55	0.26
HSV	89.17	0.27	**90.87**	**0.29**	92.61	0.17	89.81	0.27
L*a*b*	89.85	0.24	90.15	0.37	92.65	0.21	89.97	0.24
PC #3	89.82	0.21	90.15	0.37	92.64	0.18	89.87	0.21
PC #4	89.92	0.24	90.13	0.34	92.85	0.17	89.93	0.24
PC #7	**89.98**	**0.25**	89.25	0.34	**93.02**	**0.19**	**90.02**	**0.26**

(b)

	ANN		DT		SVM		KNN	
	f-measure	*Stdev*	*f-measure*	*Stdev*	*f-measure*	*Stdev*	*f-measure*	*Stdev*
RGB	48.25	1.07	61.69	1.20	69.20	1.02	60.25	1.03
HSV	58.88	0.99	**64.67**	**1.13**	67.51	0.96	61.56	1.01
L*a*b*	61.60	1.00	62.58	1.46	70.14	1.27	62.18	0.98
PC #3	61.37	0.82	62.54	1.39	69.48	0.95	61.76	0.81
PC #4	61.63	0.95	62.73	1.29	71.23	0.82	61.81	1.00
PC #7	**61.85**	**1.03**	60.00	1.24	**71.99**	**0.81**	**62.26**	**1.04**
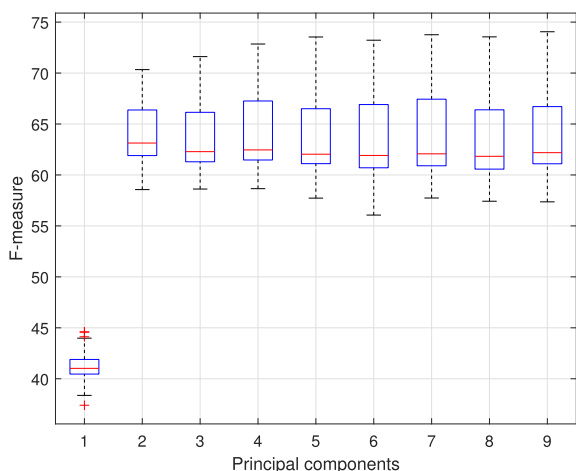
FIGURE 9. Values of the *f-measure* computed for the combined features for all color spaces using PCA.

FIGURE 10. Class-specific ROC curves of the proposed system for the classification of the ripeness level of Cape gooseberry fruits using 7 PCs with the SVM classifier.

class (i.e., each ripeness level) by employing the classifier that presented the highest performance with regard to the *accuracy* and *f-measure*. Class-specific true positives of crisp responses from each multiclass classifier were averaged over the 100 independent experimental trials; then, this average was employed as an approximation of the classification score for each class. The resulting class-specific ROC curves are shown in Figure 10.

According to Figure 10, the classification of the first four levels of ripeness (i.e., levels 1 through 4) seems to be easier than that of levels 5 through 7, as is evidenced by the higher ROC curves corresponding to the former. Particularly, the ROC curve for level 1 reaches its maximum *tpr* of approximately 85% faster than those for all the other levels. This suggests that level 1 is easier to classify up to a certain ripening stage that reaches a class overlap region in the feature space with a *false positive rate (fpr)* close to 3% and higher. On the other hand, the SVM classifier reached a higher *tpr* around 95% with a *fpr* of approximately 6% for

level 2. These findings are consistent with the observations obtained from the confusion matrices shown in Figure 6, and similar trends were acquired for all the classifiers employed in the experiments.

IV. DISCUSSION

As explained in [23] and [53], changes in the parameters L^*, a^* and b^* are associated with increases in carotenoid levels and a loss of chlorophyll in the pericarp. In this regard, Table 4 compares the mean parameter values in the $L^*a^*b^*$ color space obtained in this work with those reported by Vásquez-Parra *et al.* [5] and Puente *et al.* [54]. The differences between the $L^*a^*b^*$ parameters obtained in this research and those shown by previous studies are because

the cultivar, ripening stage or cultivation procedure for each sample was different among these studies, as was suggested by Oliveira *et al.* [14].

To evaluate the accuracy of each technique according to the color space used for a classifier, it is necessary to understand that changes in different color parameters are related to the ripening stage.

- *ANN.* This technique has already been successfully used to classify fruits according to their level of ripeness; examples of these successes can be found in the following works: Paulraj *et al.* [26], Damiri and Slamet [29], Fadilah *et al.* [33], and Shah Rizam *et al.* [40]. As shown in Table 5, the accuracies of the ANN models were significantly influenced by the chosen color space. The ANN model based on the *L*a*b** color space obtained a suitable Cape gooseberry fruit classification accuracy (89.85% ± 0.24%), which agrees with the results obtained by Fadilah *et al.* [33].

- *DT.* The DT technique was successfully used by Goel and Sehgal [37] to classify tomatoes according to their ripening stage using the *RGB* color space; this approach was capable of classifying the tomatoes with an accuracy of 94.29%. In our case, in addition to the *RGB* color space-based model, we built models for the *HSV* and *L*a*b** color spaces as well as models for their combinations with *PCA*, and we observed that the color space only slightly influences the quality of the results in terms of the *accuracy*. However, we noted an impact on the *f-measure*, which did not improve with the addition of PCs to the feature space. Thus, the performance of the *DT* classifier may be further improved by employing a better strategy for the tuning of hyperparameters.

- *SVM.* The SVM technique has been used by Xiaobo *et al.* [22] to classify apples using the *HSI* color space. In combination with the *RGB* color space, Nandi *et al.* [30] used the *SVM* to classify pieces of mango fruit. In both studies, it was possible to classify the fruits with an accuracy exceeding 95%. In our case, the best accuracies were 92.65% for the *L*a*b** color space model and 92.47% for the *RGB* color space. Further improvement was obtained by combining information from the three color spaces using 7 PCs with a final accuracy of 93.02% ± 0.19, representing the best performance obtained over all the approaches employed in this paper.

- *KNN.* Many studies have achieved results with excellent levels of accuracy; for example, Unay and Gosselin [51] classified apple stems with an accuracy reaching 99%. Regarding the problems related to the classification of fruits according to their ripening stage, Li *et al.* [27] studied the identification of blueberries at different stages of growth. Among the classification models constructed in their work, the model based on the KNN technique obtained the best accuracy (86%) using the *RGB* color space. Our results using the *L*a*b** color space showed the best accuracy (89.97% ± 0.24%),

and similar results were obtained for *RGB* and *HSV* (*RGB* = 89.55%±0.26% and *HSV* = 89.81%±0.27%). A slight improvement was obtained using 7 PCs with an accuracy of 90.02% ± 0.26%.

As shown in Table 5, the classification of Cape gooseberry fruits by their degree of ripeness is sensitive to both the color space and the classification technique used. Accordingly, the mean accuracies obtained for the *RGB*, *HSV*, and *L*a*b** color spaces were 89.46%, 90.62%, and 90.65%, respectively. These results are similar to those reported by Vélez-Rivera *et al.* [31], who used the linear discriminant analysis (LDA) classifier and found that the *RGB* and *L*a*b** color spaces present similar accuracies that are slightly higher than that obtained in the *L*u*v** color space.

Although similar techniques appear in the literature for distinct fruit classification problems, the main contributions of the paper are related to the applications of distinct pairs of color spaces and classification algorithms; the model consisting of the combination of the *L*a*b** color space with the SVM classifier provided the highest performance. To the best of the authors' knowledge, such a comparison of classifiers and color spaces is not available in the literature regarding a classification of the ripening stage of Cape gooseberry. Furthermore, information from three color spaces was fused by employing *PCA* on the nine components of the three color spaces; a superior performance was obtained with seven principal components at the expense of an increased complexity.

The proposed system was applied to real images; nevertheless, various factors, including the speed of the conveyor belt, the position of the fruit (i.e., a rotation that exposes the pedicle) and the variability of the lighting environment, which could complicate the capture of such images should be considered. Other technologies such as hyperspectral imagery may be used to identify the ripening stages of fruits. Their better discriminatory capacities notwithstanding, the application of hyperspectral imagery usually requires an increased computational complexity due to the number of bands, and thus, it may be difficult to generate the real-time responses required by production lines.

V. CONCLUSIONS

The purpose of this research was to develop a non-intrusive system for the classification of gooseberry fruits according to their degree of ripeness. Twelve classification models were developed by combining four machine learning techniques (the *ANN*, *KNN*, *DT*, and *SVM* classifiers) with three color spaces (*RGB*, *HSV*, and *L*a*b**). Additionally, a PCA strategy to combine the three color spaces was proposed, demonstrating a performance increase using 7 PCs.

The color space utilized for the classification clearly influenced the accuracy of the sorting system; this dynamic was observed mainly in the models based on the ANN and *SVM* techniques. Meanwhile, the models based on the *KNN* and *DT* techniques yielded good results regardless of the color space used. On the other hand, the models based on

the *L*a*b** color space produced good results regardless of the machine learning technique employed. However, the classifier developed from the combination of the *SVM* technique and *L*a*b** color space gave the best performance in terms of the *accuracy* and *f-measure*.

Future works should evaluate the use of different strategies (i.e., other than *PCA*) to combine information from color spaces. Information fusion techniques may involve combinations of the feature space (as *PCA*), the fusion of scores or the decisions of classifiers. These combinations may provide a better performance in the classification of fruits according to their ripeness level.

COMPETING INTERESTS

We declare that we do not have any competing interests on this manuscript.

REFERENCES

[1] M. R. Salazar, J. W. Jones, B. Chaves, and A. Cooman, "A model for the potential production and dry matter distribution of cape gooseberry *(physalis peruviana L.)*," *Sci. Horticulturae*, vol. 115, no. 2, pp. 142–148, 2008.

[2] C. L. Luchese, P. D. Gurak, and L. D. F. Marczak, "Osmotic dehydration of physalis *(physalis peruviana L.)*: Evaluation of water loss and sucrose incorporation and the quantification of carotenoids," *LWT-Food Sci. Technol.*, vol. 63, no. 2, pp. 1128–1136, 2015.

[3] T. Erkaya, E. Dağdemir, and M. Şengül, "Influence of cape gooseberry *(physalis peruviana L.)* addition on the chemical and sensory characteristics and mineral concentrations of ice cream," *Food Res. Int.*, vol. 45, no. 1, pp. 331–335, 2012.

[4] F. Ramírez, G. Fischer, T. Lee Davenport, J. C. A. Pinzón, and C. Ulrichs, "Cape gooseberry *(physalis peruviana L.)* phenology according to the BBCH phenological scale," *Sci. Horticulturae*, vol. 162, pp. 39–42, Oct. 2013.

[5] J. E. Vásquez-Parra, C. I. Ochoa-Martínez, and M. Bustos-Parra, "Effect of chemical and physical pretreatments on the convective drying of cape gooseberry fruits *(physalis peruviana)*," *J. Food Eng.*, vol. 119, no. 3, pp. 648–654, 2013.

[6] J. Benedito, S. Simal, G. Clemente, and A. Mulet, "Manchego cheese texture evaluation by ultrasonics and surface probes," *Int. Dairy J.*, vol. 16, no. 5, pp. 431–438, 2006.

[7] B. Zhang *et al.*, "Principles, developments and applications of computer vision for external quality inspection of fruits and vegetables: A review," *Food Res. Int.*, vol. 62, pp. 326–343, Aug. 2014.

[8] M. P. Arakeri and Lakshmana, "Computer vision based fruit grading system for quality evaluation of tomato in agriculture industry," *Procedia Comput. Sci.*, vol. 79, pp. 426–433, 2016. https://doi.org/10.1016/j.procs.2016.03.055

[9] K. Chen, X. Sun, C. Qin, and X. Tang, "Color grading of beef fat by using computer vision and support vector machine," *Comput. Electron. Agricult.*, vol. 70, no. 1, pp. 27–32, 2010.

[10] G. Romano, D. Argyropoulos, M. Nagle, M. T. Khan, and J. Müller, "Combination of digital images and laser light to predict moisture content and color of bell pepper simultaneously during drying," *J. Food Eng.*, vol. 109, no. 3, pp. 438–448, 2012.

[11] N. Sozer, *Imaging Technologies and Data Processing for Food Engineers*. Cham, Switzerland: Springer, 2016.

[12] T. Brosnan and D.-W. Sun, "Improving quality inspection of food products by computer vision—A review," *J. Food Eng.*, vol. 61, no. 1, pp. 3–16, 2004.

[13] W. Castro, J. Oblitas, T. Chuquizuta, and H. Avila-George, "Application of image analysis to optimization of the bread-making process based on the acceptability of the crust color," *J. Cereal Sci.*, vol. 74, pp. 194–199, Mar. 2017.

[14] S. F. Oliveira, F. J. A. Gonçalves, P. M. R. Correia, and R. P. F. Guiné, "Physical properties of *Physalis peruviana L.*," *Open Agric.*, vol. 1, no. 1, pp. 55–59, 2016.

[15] F. Avila, M. Mora, M. Oyarce, A. Zuñiga, and C. Fredes, "A method to construct fruit maturity color scales based on support machines for regression: Application to olives and grape seeds," *J. Food Eng.*, vol. 162, pp. 9–17, Oct. 2015.

[16] D. Wu and D.-W. Sun, "Colour measurements by computer vision for food quality control–A review," *Trends Food Sci. Technol.*, vol. 29, no. 1, pp. 5–20, 2013.

[17] K. León, D. Mery, F. Pedreschi, and J. León, "Color measurement in L* a* b* units from RGB digital images," *Food Res. Int.*, vol. 39, no. 10, pp. 1084–1091, 2006.

[18] R. Zakaluk and R. S. Ranjan, "Artificial neural network modelling of leaf water potential for potatoes using RGB digital images: A greenhouse study," *Potato Res.*, vol. 49, no. 4, pp. 255–272, 2006.

[19] C.-J. Du and D.-W. Sun, "Multi-classification of pizza using computer vision and support vector machine," *J. Food Eng.*, vol. 86, no. 2, pp. 234–242, 2008.

[20] Z. Arabasadi *et al.*, "Prediction and optimization of fireproofing properties of intumescent flame retardant coatings using artificial intelligence techniques," *Fire Saf. J.*, vol. 61, pp. 193–199, Oct. 2013.

[21] P. Vithu and J. A. Moses, "Machine vision system for food grain quality evaluation: A review," *Trends Food Sci. Technol.*, vol. 56, pp. 13–20, Oct. 2016.

[22] Z. Xiaobo, Z. Jiewen, and L. Yanxiao, "Apple color grading based on organization feature parameters," *Pattern Recognit. Lett.*, vol. 28, no. 15, pp. 2046–2053, 2007.

[23] S. Cárdenas-Pérez *et al.*, "Evaluation of the ripening stages of apple (golden delicious) by means of computer vision system," *Biosystems Eng.*, vol. 159, pp. 46–58, Jul. 2017.

[24] E. R. Guerrero and G. M. Benavides, "Automated system for classifying Hass avocados based on image processing techniques," in *Proc. IEEE Colombian Conf. Commun. Comput.*, Jun. 2014, pp. 1–6.

[25] F. Mendoza and J. M. Aguilera, "Application of image analysis for classification of ripening bananas," *J. Food Sci.*, vol. 69, no. 9, pp. E471–E477, 2004.

[26] M. Paulraj, C. R. Hema, K. R. Pranesh, and M. R. S. Sofiah, "Color recognition algorithm using a neural network model in determining the ripeness of a banana," in *Proc. Int. Conf. Man-Mach. Syst.* Arau, Malaysia: Univ. Malaysia Perlis, 2009, pp. 2B71–2B74.

[27] H. Li, W. S. Lee, and K. Wang, "Identifying blueberry fruit of different growth stages using natural outdoor color images," *Comput. Electron. Agricult.*, vol. 106, pp. 91–101, Aug. 2014.

[28] R. Pourdarbani, H. R. Ghassemzadeh, H. Seyedarabi, F. Z. Nahandi, and M. M. Vahed, "Study on an automatic sorting system for date fruits," *J. Saudi Soc. Agricult. Sci.*, vol. 14, no. 1, pp. 83–90, 2015.

[29] D. J. Damiri and C. Slamet, "Application of image processing and artificial neural networks to identify ripeness and maturity of the lime (Citrus medica)," *Int. J. Basic Appl. Sci.*, vol. 1, no. 2, pp. 171–179, 2012.

[30] C. S. Nandi, B. Tudu, and C. Koley, "A machine vision-based maturity prediction system for sorting of harvested mangoes," *IEEE Trans. Instrum. Meas.*, vol. 63, no. 7, pp. 1722–1730, Jul. 2014.

[31] N. Vélez-Rivera *et al.*, "Computer vision system applied to classification of 'Manila' mangoes during ripening process," *Food Bioprocess Technol.*, vol. 7, no. 4, pp. 1183–1194, 2014.

[32] H. Zheng and H. Lu, "A least-squares support vector machine (LS-SVM) based on fractal analysis and CIELab parameters for the detection of browning degree on mango *(Mangifera indica L.)*," *Comput. Electron. Agricult.*, vol. 83, pp. 47–51, Apr. 2012.

[33] N. Fadilah, J. Mohamad-Saleh, Z. A. Halim, H. Ibrahim, and S. S. S. Ali, "Intelligent color vision system for ripeness classification of oil palm fresh fruit bunch," *Sensors*, vol. 12, no. 10, pp. 14179–14195, 2012.

[34] E. Elhariri, N. El-Bendary, A. M. M. Hussein, A. E. Hassanien, and A. Badr, "Bell pepper ripeness classification based on support vector machine," in *Proc. Int. Conf. Eng. Technol. (ICET)*, Apr. 2014, pp. 1–6.

[35] V. Mohammadi, K. Kheiralipour, and M. Ghasemi-Varnamkhasti, "Detecting maturity of persimmon fruit based on image processing technique," *Sci. Horticulturae*, vol. 184, pp. 123–128, Mar. 2015.

[36] N. El-Bendary, E. El Hariri, A. E. Hassanien, and A. Badr, "Using machine learning techniques for evaluating tomato ripeness," *Expert Syst. Appl.*, vol. 42, no. 4, pp. 1892–1905, Mar. 2015.

[37] N. Goel and P. Sehgal, "Fuzzy classification of pre-harvest tomatoes for ripeness estimation—An approach based on automatic rule learning using decision tree," *Appl. Soft Comput.*, vol. 36, pp. 45–56, Nov. 2015.

[38] G. Polder, G. W. A. M. van der Heijden, and I. T. Young, "Spectral image analysis for measuring ripeness of tomatoes," *Trans. ASAE*, vol. 45, no. 4, p. 1155, 2002.

[39] A. Rafiq, H. A. Makroo, and M. K. Hazarika, "Artificial neural network-based image analysis for evaluation of quality attributes of agricultural produce," *J. Food Process. Preservation*, vol. 40, no. 5, pp. 1010–1019, 2016.

[40] M. S. B. S. Rizam, A. R. F. Yasmin, A. I. M. Yassin, and K. Shazana, "Non-destructive watermelon ripeness determinationusing image processing and artificial neural network(ANN)," *Int. J. Elect. Comput. Eng.*, vol. 3, no. 2, pp. 332–336, 2009.

[41] F. Pedreschi, J. León, D. Mery, and P. Moyano, "Development of a computer vision system to measure the color of potato chips," *Food Res. Int.*, vol. 39, no. 10, pp. 1092–1098, 2006.

[42] W. Castro, J. Oblitas, J. Maicelo, and H. Avila-George, "Evaluation of expert systems techniques for classifying different stages of coffee rust infection in hyperspectral images," *Int. J. Comput. Intell. Syst.*, vol. 11, no. 1, pp. 86–100, 2018.

[43] K. Bravo and E. Osorio, "Characterization of polyphenol oxidase from cape gooseberry *(physalis peruviana L.)* fruit," *Food Chem.*, vol. 197, pp. 185–190, Apr. 2016.

[44] G. Fischer, D. Miranda, W. Piedrahita, and J. Romero, "Avances en cultivo, poscosecha y exportación de la uchuva *(Physalis peruviana L.)* en Colombia," Univ. Nacional de Colómbia, Colómbia, Bogotà, Tech. Rep. CDD-21 634.7/2005, 2005.

[45] J. Blasco, N. Aleixos, J. Gómez, and E. Moltó, "Citrus sorting by identification of the most common defects using multispectral computer vision," *J. Food Eng.*, vol. 83, no. 3, pp. 384–393, 2007.

[46] P. K. Dash, S. Mishra, and G. Panda, "A radial basis function neural network controller for UPFC," *IEEE Trans. Power Syst.*, vol. 15, no. 4, pp. 1293–1299, Nov. 2000.

[47] C. Kong *et al.*, "Quality changes and predictive models of radial basis function neural networks for brined common carp *(Cyprinus carpio)* fillets during frozen storage," *Food Chem.*, vol. 201, pp. 327–333, Jun. 2016.

[48] M. H. Beale, M. T. Hagan, and H. B. Demuth, *Neural Network Toolbox User's Guide*. Natick, MA, USA: The MathWorks, 2012, pp. 201–213.

[49] S. R. Safavian and D. Landgrebe, "A survey of decision tree classifier methodology," *IEEE Trans. Syst., Man, Cybern.*, vol. 21, no. 3, pp. 660–674, May/Jun. 1991.

[50] L. Breiman, J. H. Friedman, R. A. Olshen, and C. J. Stone, *Classification and Regression Trees*. London, U.K.: Chapman & Hall, 2017.

[51] D. Unay and B. Gosselin, "Stem and calyx recognition on 'Jonagold' apples by pattern recognition," *J. Food Eng.*, vol. 78, no. 2, pp. 597–605, 2007.

[52] X. Deng, Q. Liu, Y. Deng, and S. Mahadevan, "An improved method to construct basic probability assignment based on the confusion matrix for classification problem," *Inf. Sci.*, vol. 340, pp. 250–261, May 2016.

[53] R. A. Itle and E. A. Kabelka, "Correlation between L*a*b* color space values and carotenoid content in pumpkins and squash *(Cucurbita spp.)*," *HortScience*, vol. 44, no. 3, pp. 633–637, 2009.

[54] L. A. Puente, C. A. Pinto-Muñoz, E. S. Castro, and M. Cortés, "Physalis peruviana linnaeus, the multiple properties of a highly functional fruit: A review," *Food Res. Int.*, vol. 44, no. 7, pp. 1733–1740, 2011.

JIMY OBLITAS received the master's degree in science and a specialization in operations management. He is currently pursuing the Ph.D. degree with the University of Lleida, Spain, where he is also an Agroindustrial Engineer. He has executive experience in the planning and development of projects, managing the Center for Research and innovations for the Peruvian Agroindustry.

MIGUEL DE-LA-TORRE received the Ph.D. degree from the École de Technologie Supérieure, in 2015. Since 2006, he has been a full-time Teacher and a Researcher with the Department of Computer Science and Engineering, University of Guadalajara. As a member of the Computer Science Academy, he collaborates in graduate and undergraduate engineering programs at the University Center of Los Valles. His research interests include adaptive pattern recognition, signal, and image processing applied to biometrics, scene analysis and understanding, food engineering, and satellite imagery. Since 2017, he has been a Distinguished National Researcher at the National System of Researchers, Mexico.

CARLOS COTRINA graduated from the Universidad Privada del Norte, Peru, where he is currently an Industrial Engineer. His research interests include modeling and optimization in food processing.

KAREN BAZÁN graduated from the Universidad Privada del Norte, Peru, where she is currently an Industrial Engineer. Her research interests include modeling and optimization in image analysis for applications in automated food engineering.

WILSON CASTRO received the M.Sc. degree in science and engineering of food and the Ph.D. degree in food science, technology, and management from the Universitat Politècnica de València, Spain. He is currently a Senior Researcher Professor with the Department of Industrial Engineering, Universidad Privada del Norte, Peru. He is also a Principal Investigator and a Collaborative Researcher in different research projects above the applications of images, pattern recognition, artificial intelligence, and software development to the analysis of agri-food products.

HIMER AVILA-GEORGE (SM'18) received the Ph.D. degree in computer science from the Universitat Politècnica de València, Spain. He was a Researcher and the Academic Manager in various universities in Mexico. He is currently a Full Professor with the University of Guadalajara, Mexico. In consideration of his professional career, since 2014, he has been a distinguished National Researcher (Level I) at the National System of Researchers, Mexico. His current research interests include combinatorial optimization, software engineering, and machine learning.

• • •